IJE TRANSACTIONS B: Applications Vol. 39, No. 02, (February 2026) 321-340

International Journal of Engineering

Journal Homepage: www.ije.ir

Dynamic Performance and Added Resistance of Duisburg Test Case Ship Using Hybrid CFD- Strip Theory Method

M. Ahmadi, M. Yousefifard*, H. Nowruzi

Marine Technology Research Group, Department of Mechanical Engineering, Babol Noshirvani University of Technology, Babol, Iran

P A P E R I N F O

Paper history:
Received 10 January 2025
Received in revised form 20 February 2025
Accepted 07 March 2025

Keywords:
Dynamic Response
Added Resistance
Duisburg Test Case Ship
Computational Fluid Dynamics
Strip Theory

A B S T R A C T

To predict the ship's behavior in the real sea state, it is important to know its dynamic responses and added resistance in different physical and environmental conditions. Therefore, the current study employs the hybrid CFD-strip theory method to study the added resistance and dynamic responses (i.e., heave and pitch RAOs) of the DTC hull. For this purpose, different wavelengths and directions and various ship drafts and trims were considered as defined physical and environmental parameters. In addition, for the CFD approach, the finite volume method (FVM) using open source software of OpenFOAM was used, while the strip theory method was applied using Tribon. The results of the CFD and strip theory have been validated against the published experimental and numerical data, and an acceptable accordance was achieved. The obtained results indicate that an enhancement in incident wave angles increases heave and pitch RAOs. Moreover, draft change has a non-uniform effect on heave RAO, while draft reduction causes higher pitch RAO. An increase in trim by aft results in higher heave RAO. Moreover, an enhancement in trim by the bow increases the pitch RAO. Finally, the highest added resistance is achieved at the head sea for the small draft of T= 12 m and trim by bow 0.6 ° in case of wavelength equal to ship length.

***doi**: 10.5829/ije.2026.39.02b.04*

Graphical Abstract

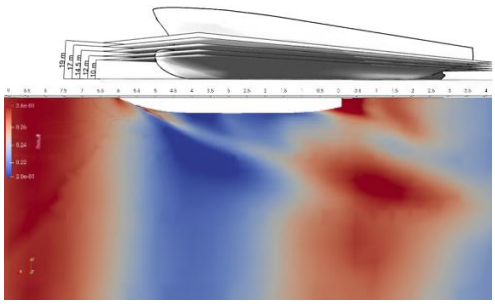

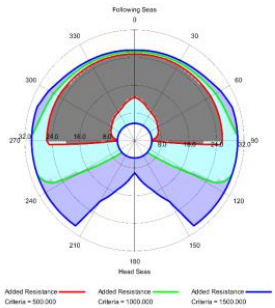

NOMENCLATURE

C_B	Block Coefficient (-)	U_g	Grid cell velocity (m/s)
F_{Gi}	Gravitational force (N)	U_r	Fluid domain velocity (m/s)
F_{Hsi}	Hydrostatic force (N)	v	Ship velocity (m/s)
$I5$	Moment of inertia for pitch motion (kg·m^2)	**Greek Symbols**	
LPP	Length between perpendiculars (m)	α	Volume ratio (-)
M	Ship Mass (kg)	ω	Rigid body angular velocity (rad/s)
P_d	Dynamic pressure (N/m^2)	ρ	Fluid density (kg/m^3)
$\bar{R}_{aw}$	Average Added Resistance (N)		
U	Fluid velocity (m/s)		

*Corresponding Author Email: yousefifard@nit.ac.ir (M. Yousefifard)

Please cite this article as: Ahmadi M, Yousefifard M, Nowruzi H. Dynamic Performance and Added Resistance of Duisburg Test Case Ship Using Hybrid CFD- Strip Theory Method. International Journal of Engineering, Transactions B: Applications. 2026;39(02):321-40.

1. INTRODUCTION

One of the vital components of the global economy is the shipping industry. Maritime transportation accounts for about 2.5% of the global total CO_2 emissions, despite carrying out more than 80% of international trade volume by sea. Therefore, the International Maritime Organization (IMO) has considered the requirements to reduce these emissions by 50% for 2050. One of the basic strategies for achieving the IMO indicators is to improve the ship's hydrodynamic performance. Since added resistance directly impacts ship efficiency, an accurate prediction of seakeeping performance is crucial in ship design. Additionally, the importance of seakeeping analysis of merchant ships has increased due to market demands and recent international regulations, as evidenced by the relevant activities of ITTC (1).

Research institutes have introduced and tested different standard hull forms for merchant ships, including Wigley, DTMB, the S175, and KCS hulls. More recently, the Duisburg Test Case (DTC) containership was introduced to the public (2), which is also considered in the present study. According to the literature review, one can find comprehensive experimental studies (3-10) on the resistance and seakeeping of standard hull forms both in calm water and conditions in waves. For example, in 2015, Park et al. (3) conducted some experimental tests on motion response and added resistance for the KVLCC2 hull in head waves. They highlighted the fundamental uncertainties in their experimental measurements. Sprenger et al. (5) conducted experimental studies on the added resistance and maneuverability of three ship hulls: the KVLCC2, DTC, and RoPax ferry. They conducted their study under various wave conditions. In 2020, Liu et al. (7) conducted an extensive experimental and numerical investigation on the added resistance and seakeeping behavior of the DTC hull. They predicted the thrust forces at various wave angles and the ship's velocities. In 2023, Chirosca et al. (10) investigated the added resistance and seakeeping of the DTC hull in head waves, both experimentally and numerically. They found strong concordance between their numerical simulations and experimental results.

However, the importance of CFD simulations and fast and sufficiently accurate methods like strip theory is growing in the study of added resistance and seakeeping of standard hull forms in head and oblique waves (11-32). For example, in 2013, Sadat-Hosseini et al. (12) numerically predicted the added resistance and seakeeping of the KVLCC2 hull in head waves using CFD simulation. They investigated the effects of short and long head waves on surge and pitch motions. Moctar et al. (16) conducted a numerical study on the added resistance and seakeeping of the DTC hull in 2016. They demonstrated that short wave-dominated diffraction could lead to numerical diffusion. In 2018, Liu et al. (21) used the open-source CFD code of OpenFOAM to simulate the added resistance and seakeeping of the DTC hull in short and long head wave conditions. Only at high hull velocity did they demonstrate an appropriate accordance between the CFD results and the experiment. In 2021, Chirosca and Gasparotti (26) predicted the resistance, sinkage, and trim of the DTC hull using ANSYS commercial software, and they found proper accordance between their CFD results and experiment. Recently, in 2023, Fang et al. (31) investigated the drift force and seakeeping of the DTC hull under oblique and head waves using CFD simulations. They demonstrated the reliability of their CFD model in a manner that was in acceptable agreement with the experimental results. Despite the special role of experimental and numerical studies, the semi-empirical formulation also plays an interesting role in studying the resistance and seakeeping of standard hull forms (33-35). Table 1 tabulates a summary of the cited works.

TABLE 1. summary of the cited works

Reference	Year	Methodology	Ship type	Details of the study
Guo et al. (11)	2012	CFD (RANS)	KVLCC2	- Added resistance and seakeeping - Head waves
Sadat-Hosseini et al. (12)	2013	CFD (URANS)	KVLCC2	- Added resistance and seakeeping - Short and long head waves
Gasparotti and Rusu (13)	2013	Strip theory	containership	- Seakeeping - Wave condition of specific sea area of the black sea
Park et al. (3)	2015	Experimental	KVLCC2	- Added resistance and seakeeping - Head waves
Liu and Papanikolaou (14)	2016	Potential flow	Bulk carrier	- Added resistance - Different wave headings
Park et al. (4)	2016	Experimental and strip theory	KVLCC2	- Added resistance and seakeeping - Different draft conditions - Head waves

Islam and Akimoto (15)	2016	CFD (RANS)	KVLCC2	- Calm water and added resistance - Head waves
Moctar et al. (16)	2016	CFD (RANS)	DTC	- Added resistance and seakeeping - Head waves
Liu et al. (33)	2016	Semi-empirical Formula	VLCC	- Added resistance - Head waves
Sprenger et al. (5)	2016	Experimental	KVLCC2 DTC RoPax ferry	- Added resistance - Maneuvering - Adverse conditions
Papanikolaou et al. (17)	2016	CFD (RANS)	DTC KVLCC2	- Maneuvering - Adverse conditions
He et al. (18)	2016	CFD (RANS)	DTC	- Sinkage and trim - Ship-bottom interaction
Liu et al. (19)	2017	CFD	DTC	- Seakeeping - Oblique waves
Liu and Papanikolaou (34)	2017	Semi-empirical Formula	DTC KVLCC2	- Added resistance and powering - Head waves
Lee et al. (36)	2017	Potential flow	DTC KVLCC2	- Added resistance and seakeeping - Head waves
Liu et al. (20)	2018	CFD	DTC	- Seakeeping - Oblique waves
Liu et al. (21)	2018	CFD	DTC	- Added resistance and seakeeping - Short and long head waves
Park et al. (6)	2019	Experimental and strip theory	S-VLCC	- Added resistance - Oblique waves
Srivastava et al. (22)	2019	CFD (RANS)	DTC	- Resistance in calm water - Free surface
Islam and Soares (23)	2019	CFD	KCS DTC KVLCC2 JBC	- Resistance in calm water - Sinkage and trim
Martic et al. (24)	2019	CFD (RANS)	DTC	- Added resistance - Shallow water
Liu et al. (7)	2020	Experimental and CFD	DTC	- Added resistance, seakeeping and prediction of propulsion - Regular head waves
Deng et al. (25)	2020	CFD	DTC KVLCC2	- Resistance and squat - Shallow water
Kianaci et al. (8)	2020	Experimental and CFD	DTC	- Resistance and Maneuvering - Calm water
Chirosca and Gasparotti (26)	2021	CFD	DTC	- Resistance, sinkage and trim - Calm water
Amini-Afshar and Bingham (37)	2021	Strip theory	Wigley ULYSSES KVLCC2 DTC	- Added resistance and drift force - Head waves
Lee et al. (9)	2021	Experimental and CFD	S-LNGC S-VLCC H-CNTR K-Supramax	- Added resistance and seakeeping - Oblique waves
Amini-Afshar (27)	2021	BEM and Green function	Wigley TypeI ULYSSES KVLCC2 DTC	- Added resistance - Proposed Salvesen–Tuck–Faltinsen (STF) strip theory

Kobayashi et al. (28)	2021	CFD (RANS)	JBC DTC	- Added resistance and seakeeping - Head waves
Song et al. (38)	2022	Rankine panel method	Wigley S-175 KVLCC2	- Added resistance - Regular head waves
Mikkelsen et al. (29)	2022	CFD	KCS	- Added resistance and seakeeping - Oblique waves
Islam et al. (35)	2022	CFD and Semi-empirical Formula	KCS DTC VLCC	- Resistance and prediction of population - Calm water
Kinaci and Ozturk (30)	2022	CFD	DTC	- Maneuverability - Calm water
Chirosca et al. (10)	2023	Experimental and CFD	DTC	- Added resistance and seakeeping - Head waves
Fang et al. (31)	2023	CFD	DTC	- Drift force and seakeeping - Oblique and head waves
Chowdhury et al. (32)	2023	CFD	KVLCC2	- Added resistance and seakeeping - Head and beam waves

Based on our best knowledge and the cited papers in Table 1, the DTC ship is still considered a relevant case for conducting numerical and experimental analyses. The increasing adoption of container ship hull designs is the primary factor contributing to this trend. Also, the lack of comprehensive investigations into the added resistance and seakeeping of DTC hull under different drafts and trims is evident. Furthermore, it is necessary to examine the effects of the wavelength and wave direction on the added resistance and seakeeping of the DTC hull. Moreover, a hybrid model of CFD-strip theory to predict the added resistance and seakeeping of the DTC hull under various geometrical and environmental conditions has not been suggested so far. Therefore, the primary goal of this study is to conduct a thorough investigation into the added resistance and seakeeping of the DTC hull under various geometrical and environmental conditions, utilizing the CFD-strip theory to evaluate the precise performance of this method in different conditions. To this accomplishment, the open-source software of OpenFOAM is used for the CFD simulations, and the strip theory method is employed using Tribon software. This study has been performed using OpenFOAM-dev on Ubuntu 17.04. In addition, heave and pitch RAOs (as seakeeping criteria) and the added resistance of DTC hulls with various drafts and trims are studied under different wavelengths and wave directions. Finally, some phenomenological studies are conducted to assess the fluid flow behavior around the considered DTC hull.

The current paper is structured as follows: Section 2 presents the conducted physics of the problem and the numerical procedure. Section 3 provides the validation studies in both calm water and wavy conditions. Section 4 presents the results and discusses the added resistance and seakeeping of the DTC hull under various geometrical and environmental conditions. Finally, section 5 presents the major conclusions.

2. PHYSICS OF THE PROBLEM AND NUMERICAL PROCEDURE

2. 1. Governing Equations This study considers a hybrid model combining two numerical approaches, i.e., computational fluid dynamics (CFD) and strip theory. In the CFD approach, the Finite Volume Method (FVM) scheme uses Reynolds averaged Navier Stokes (RANS) equations to simulate fluid flow. Additionally, a two-phase method employing the volume of fraction (VOF) and artificial density (23) models the free surface, utilizing the open-source software OpenFOAM. The equations for the conservation of mass and momentum in two-phase fluid motion are as follows:

$$\nabla.U = 0 \tag{1}$$

$$\frac{\partial \rho U}{\partial t} + \nabla \cdot \left(\rho\left(U - U_g\right)U\right) = -\nabla p_d - g \cdot \mathrm{x}\nabla\rho + \nabla \cdot \left(\mu_{eff}\nabla U\right) + \left(\nabla U\right)\cdot\nabla\mu_{eff} + f_\sigma \tag{2}$$

here, U and U_q are fluid and grid cell velocities [m/s], respectively. Moreover, P_d is the dynamic pressure and ρ is the fluid density [kg/m^3]. The acceleration of gravity is shown by g, $\mu_{\mathrm{eff}} = \rho(\mathrm{v_t} + \mathrm{v})$ as the effective dynamic viscosity, and $\mathrm{f}_\sigma = \sigma \mathrm{k} \nabla \alpha$ is the source term (where k is the curvature of the free surface and σ = 0.07 [kg/sq.s] is the surface tension). The free surface is also predicted using VOF as follows:

$$\frac{\partial \alpha}{dt}+\nabla\cdot\left[\left(U-U_g\right)\alpha\right]+\nabla\cdot\left[U_r\left(1-\alpha\right)\alpha\right]=0$$
$$\begin{cases}\rho=\alpha\rho_1+\left(1-\alpha\right)\rho_g\\ \mu=\alpha\mu_1+\left(1-\alpha\right)\mu_g\end{cases} \quad (3)$$
$$\begin{cases}\alpha=0 & air\\ \alpha=0 & water\\ 0<\alpha<1 & \text{int}erface\end{cases}$$

where, the variable of α is the volume ratio, and U_r is the fluid domain velocity (24). Notably, that the shear stress transport (SST) equation is also considered for the simulation of turbulent flow (7). The governing equations on the translational and rotational rigid body motions of the considered ship are as follows:

$$M\frac{dV}{dt}=f \quad (4)$$

$$m\frac{d\omega}{dt}+\omega\times m\omega=n \quad (5)$$

here, *V* shows the velocity of the ship's center of mass, *m* is the tensor of the moment of inertia, ω is the rigid body angular velocity, and *n* is the excitation force applied to the ship body.

In the strip theory method, based on the potential flow function using Tribon software, the ship's motions are considered linear and harmonic in regular sinusoidal waves. In this approach, the linearized differential equations for ship motions are expressed as follows (8, 25):

$$\sum_{k=1}^{6}\left[\left(M_{jk}+A_{jk}\right)\ddot{\eta}_k+B_{jk}\dot{\eta}_k+C_{jk}\eta_k\right]=F_{Gi}+F_{HSi}+F_je^{i\omega t}\quad .\quad j=1\ldots.6 \quad (6)$$

where, *J* and *k* are indices of motion, M_{jk} is the mass matrices, A_{jk} is the added mass, B_{jk} , and C_{jk} are damping coefficient, and hydrostatic restoring coefficient, respectively. The variables of F_{Hsi}, FGj and $F_je^{i\omega t}$ are hydrostatic force, gravitational force and driving force, respectively. In addition, $\ddot{\eta}_k$ ،$\dot{\eta}_k$ and η_k are respectively the acceleration, velocity, and amplitude of the kth response as follows (8):

$$\eta_k(t)=\bar{\eta}_ke^{i\omega_et}=|\bar{\eta}_k|e^{i\sigma_k}e^{i\omega_t t}=|\bar{\eta}_k|e^{i(\omega_et+\sigma_k)} \quad (7)$$

The encounter frequency is ω_e, the unit of the imaginary number is $i=\sqrt{-1}$, and $\bar{\eta}_k$ is the complex amplitude of the kth response as follows:

$$\bar{\eta}_k=\bar{\eta}_{kR}+i\bar{\eta}_{kI}=|\bar{\eta}_k|e^{i\sigma_k} \quad (8)$$

where, $|\bar{\eta}_k|$and σ_k are the magnitude and the phase angle of the response, respectively. For the couple of heave and pitch motions, the time-dependent equations are as follows:

$$\begin{aligned}&(M+A_{33}(t))\ddot{\eta}_3+B_{33}(t)\dot{\eta}_3+A_{35}(t)\ddot{\eta}_5+B_{35}(t)\dot{\eta}_5=F_{G3}+F_{HS3}(t)+F_3(t)e^{i\omega t}\\ &A_{53}(t)\ddot{\eta}_3+B_{53}(t)\dot{\eta}_3+\left(I_5+A_{55}(t)\right)\ddot{\eta}_5+B_{55}(t)\dot{\eta}_5=F_{G5}+F_{HS5}(t)+F_5(t)e^{i\omega t}\end{aligned} \quad (9)$$

here, the ship's mass is *M* [kg] and I_5 is the moment of inertia for pitch motion. In the current study, added mass and damping coefficients are calculated using the the Frank close-fit method on the wet surface of the ship's hull (37). In Frank Close-fit method, the effects of surface tension and non-linear free surface conditions, kinematic boundary conditions and Bernoulli equations are ignored (9).

According to Amini-Afshar (27), the time series responses of a ship in the sea with long waves can be obtained using the following algorithm (28, 38):

$$\begin{aligned}&\eta_i(t)=\sum_{n=1}^{N}\bar{\zeta}_n|H_i(\omega_{e\,n})|\,cos(\,\omega_{e\,n}t+\sigma_{i.n}+\varepsilon_n)\quad for\quad i=1.2.3\\ &\eta_i(t)=\sum_{n=1}^{N}\bar{\zeta}_n|H_i(\omega_{e\,n})|\,k_n\,cos(\,\omega_{e\,n}t+\sigma_{i.n}+\varepsilon_n)\quad for\quad i=4.5.6\end{aligned} \quad (10)$$

where, $\bar{\zeta}_n$ is the wave height, ε_n is the random phase change angle, k_n is the wave number, the response amplitude operator (RAO) is denoted by Hi, and the phase change angle of the desired response part is shown by $\sigma_{i.n}$. Notably, for calculating the hull resistance in calm water, the Holtrop and Mennen method has been used.

The strip theory method also numerically analyzes the added resistance. This approach employs the conservation of motion method, which is based on band theory in the frequency domain. There are various methods for analyzing the added resistance in the frequency domain. Among them, Maruo's momentum conservation method is used as follows (39):

$$R_{aw}=\frac{1}{4\pi k_0}\left[-\int_{-\infty}^{k_1}+\int_{k_2}^{k_3}+\int_{k_4}^{\infty}|H(k)|^2\frac{v(k)\{k-k_0\,cos\,\beta\}}{\sqrt{v^2(k)-k^2}}\right]\,dk \quad (11)$$

where:

$$\begin{aligned}&k_0=\frac{{\omega_0}^2}{g}\ ,\ \ \tau=U\omega/g\\ &v(k)=\frac{(\omega+kU)^2}{g}=K+2\tau k+\frac{k^2}{K_0}\ ,\\ &K=\frac{\omega^2}{g}\ ,\ \ K_0=\frac{g}{U^2}\\ &k_1\,,k_2=-\frac{K_0}{2}\left(1+2\tau\pm\sqrt{1+4\tau}\right)\ ,\\ &k_3\,,k_4=\frac{K_0}{2}\left(1-2\tau\pm\sqrt{1-4\tau}\right)\end{aligned} \quad (12)$$

here, *H(k)* is the Kochin function as follows:

$$H^{\pm}(k) = \iint \left(\frac{\partial \varphi}{\partial n} - \varphi \frac{\partial}{\partial n}\right) e^{-k\chi \pm i\varepsilon_k \eta\sqrt{K^2-k^2}+ik\zeta} ds(\chi,\eta,\zeta) = C(k) \pm i\varepsilon_k S(k) \quad (13)$$

where ε_k represents the sign of (ω+ kU) as follows:

$$\varepsilon_k = sgn(\omega + kU) \quad (14)$$

As may be seen in Equation 13, the Kochin function has as a symmetric and an asymmetric component. These components can be expressed as follows:

$$|H(k)|^2 = |C(k)|^2 + |S(k)|^2 \quad (15)$$

where, *C(k)* and *S(k)* are:

$$\begin{cases} C(k) = C_7(k) - \frac{\omega\omega_0}{g}\sum_{j=1,3,5}\frac{x_j}{a}C_j(k) \\ S(k) = S_7(k) - \frac{\omega\omega_0}{g}\sum_{j=2,4,6}\frac{x_j}{a}S_j(k) \end{cases} \quad (16)$$

The parameters of $C_j(k)$ and $S_j(k)$ in Equation 16 are as follows:

$$\begin{cases} C_j(k) = \iint \left(\frac{\partial \varphi_j}{\partial n} - \varphi_j \frac{\partial}{\partial n}\right) e^{-k\chi+ik\zeta}\cos(\eta\sqrt{K^2-k^2})ds \ , \ (j = 1,2,\dots,7) \\ S_j(k) = \iint \left(\frac{\partial \varphi_j}{\partial n} - \varphi_j \frac{\partial}{\partial n}\right) e^{-k\chi+ik\zeta}\sin(\eta\sqrt{K^2-k^2})\, ds \ , \ (j = 1,2,\dots,7) \end{cases} \quad (17)$$

here, the velocity potential satisfies the following boundary condition:

$$\frac{\partial \varphi_j}{\partial n} = n_j + \frac{U}{i\omega}m_j \ \ (j = 1,2,\dots,6) \ \ = \frac{\partial \varphi_I}{\partial n} \ \ (j = 7) \quad (18)$$

$$\begin{cases} (n_1,n_2,n_3) = \vec{n} \\ (m_1,m_2,m_3) = -(\vec{n}\,.\nabla)\vec{U} \\ (n_4,n_5,n_6) = \vec{r}\times\vec{n} \\ (m_4,m_5,m_6) = -(\vec{n}\,.\nabla)(\vec{r}\times\vec{U}) \end{cases} \quad (19)$$

where U is the ship velocity and ϕ_1 is the velocity potential of the incident wave. Therefore, using the velocity potential obtained from the strip theory, the Kochin function is calculable. Then, it is possible to find the added resistance using Equation 11.

In an irregular seaway, added resistance is the time mean value of the second-order wave force (as superposition of the regular wave responses). Therefore, the average added resistance has following form (16):

$$\bar{R}_{aw} = 2\int_0^{\infty} R(\omega)\, S_\zeta(\omega) d\omega \quad (20)$$

here, $R(\omega)$ is the mean added resistance function in regular waves and $S_\zeta(\omega)$ is the spectral density function of the irregular seaway. Therefore, almost all available methods to calculate added resistance in waves focus on the regular waves. However, the added resistance in regular waves varies linearly with wave height squared as follows:

$$R(\omega) = R_{aw}/\zeta_a^2 \quad (21)$$

here ζ_a is the wave amplitude.

2. 2. Physics of the Problem In this study, the Duisburg Test Case (DTC) ship hull (2) is considered. It is intended to use both a full-scale and a scaled model in the hybrid CFD-strip theory method. Indeed, the full-scale model is used in strip theory calculations, while the model scale of 1:59.407 is considered for CFD simulations. Table 2 shows the main specifications of the DTC hull. Figure 1 shows the schematic of the DTC ship's hull.

TABLE 2. Main characteristics of the DTC hull

Geometrical Characteristics	Variable	Model	Full scale	Unit
Scale factor	λ	1:59.407	[-]	[-]
Length between perpendiculars	L_{PP}	5.976	355	[m]
Waterline breadth	B_{WL}	0.859	51	[m]
Design draft	T	0.244	14.5	[m]
Volume displacement	∇	0.824	173468	[m^3]
Wetted surface	S_w	1.209	22032	[m^2]
Block coefficient	C_B	0.661	0.661	[-]
Design speed	V	1.68	12.86	[m/s]
Longitudinal center of gravity—from aft perpendicular	X_{CG}	2.929	174.059	[m]
Vertical center of gravity—from aft perpendicular	Z_{CG}	0.334	19.851	[m]
Radius of gyration	r_{yy}	1.471	87.4	[m]

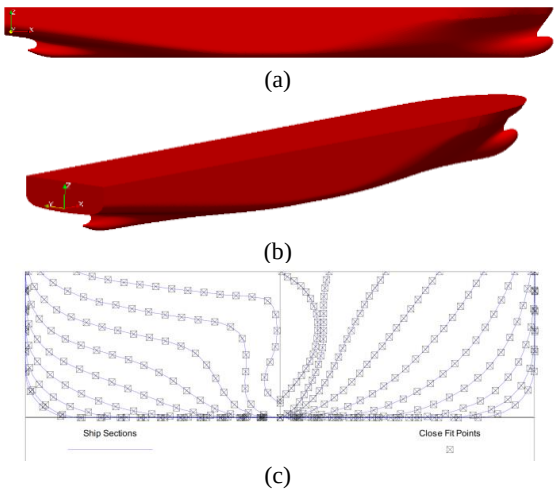

(a) (b) (c)

Figure 1. Schematic of DTC ship hull geometry: (a) profile view, (b) 3D view and (c) points matched on the body using the Close-Fit method

Figure 2 displays the used 3D model and the computational domain of the current study. The dimensions of the computational domain were selected based on the recommended values provided by ITTC (1) for CFD methods and corroborated by similar studies, as illustrated in Figure 2(c). The wave generator is placed at x = 10 m, and the wave propagation direction is in the negative direction of the x-axis. The symmetry boundary condition is used, and only half of the ship's hull was simulated in the OpenFOAM. The water line is located at z=0.244 m, and the ship center of mass is located at x=2.929 m, y=0 m, z=0.2 m.

Also, the settings related to the numerical solution and physical constants of the problem are presented in Table 3. In addition, more details of the boundary conditions can be seen in Table 4. As can be seen in Table 3, the SST k-ω turbulence model was used in this study. This model is well-suited for simulating ship hydrodynamics due to its ability to resolve complex flow physics such as interaction with free-surface waves. Due to hybrid formulation in this model (i.e., k-ω equations near the wall and the k-ε formulation in free-stream regions), it has accuracy in Adverse Pressure Gradients (40) and Robustness Near-Wall Treatment (41). Moreover, this turbulence model is recommend by ITTC (42) and has been extensively validated for ship flows, including benchmark cases like tanker and DTMB 5415 combatant (43).

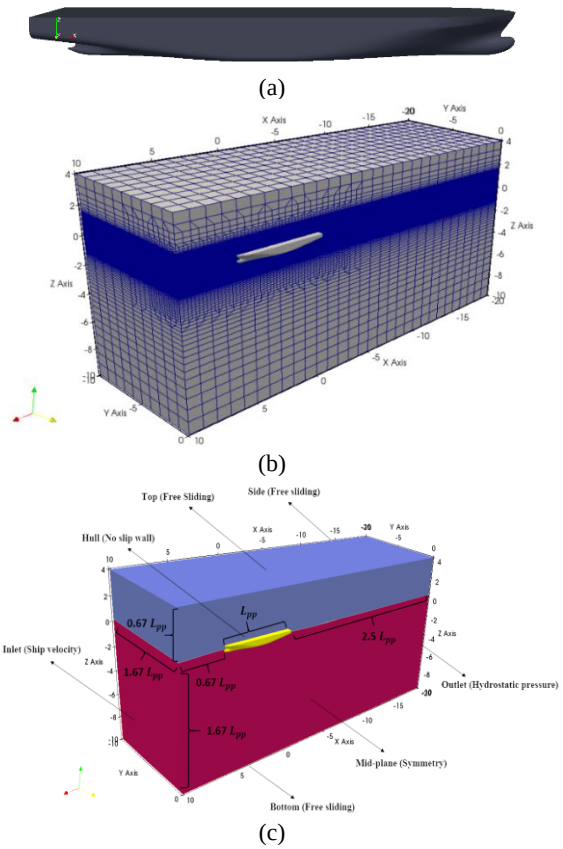

Figure 2. Schematic of (a) 3D model of the DTC, (b) computational domain, and (c) boundary conditions

TABLE 3. Numerical solution settings and Value of physical properties

Parameter	Setting
Solver	interDyMFoam, unsteady, two phase flow, dynamic mesh
Viscous model	SST k-ω
Free surface scheme	VOF
Convective acceleration discretization method	Second-order upwind
Initial time step	0.0001 [s]
Dynamic viscosity (υ)	1×10^{-6} [m^2 /s]
Water density (ρ)	998 [kg/m^3]
Surface tension (σ)	0.07 [N/m]

TABLE 4. Boundary conditions

Boundary	Type
Inlet	Velocity inlet
Outlet	Pressure outlet
Side walls	Symmetry
Top & Bottom	Free slip
Body	No slip

Also, considering the importance of computational cost and the low importance of surface tension effects, and considering the dimensions of the problem, using the VOF method is more justified to this research.

2. 3. Hybrid Solution Algorithm Ship dynamic analysis is possible in several ways; experimental, numerical (CFD), and strip theory methods are the most important methods. Each of these methods has its advantages and disadvantages. For instance, using the experimental method comes with significant costs and numerous limitations. Also, numerical methods have many limitations for simulating the real environment of the sea. The simulation of the ship using original dimensions, the analysis of ship dynamics in irregular waves, and the application of different wave angles are some of the limitations of the numerical method. The strip theory method has numerous limitations. Some of the most important limitations of using the strip theory method are:

- The conditions of the waves must be within the validity range of the linear wave theory. (small amplitude waves)
- The length-to-beam ratio of the ship should be very large. (slender body)

- There must be a limit to the ship's range of motion. (linear motion)
- The ship is considered to have a rigid and wall-sided hull.
- The presence of the hull does not affect the waves.

Many of these limitations are caused by the methods used in the hydrodynamic analysis of ship sections in the strip theory method. In the field of hydrodynamics, numerical methods based on the finite volume method (FVM) possess greater power. This means that by incorporating the numerical solution results into the hydrodynamic analysis used in the strip theory, many of the limitations of the strip theory method can be overcome. Therefore, the current study proposes a hybrid of CFD-strip theory, and Figure 3 depicts its solution flowchart.

3. VALIDATION STUDIES

Preliminary mesh sensitivity analysis is conducted, and the total mesh of 705,000 cells is selected. Figure 4 illustrates the mesh structure in the main domain and around the hull. In this study, a non-uniform structured mesh has been used in a large part of the solution domain to obtain the highest performance in the numerical solution. In this study, the computational domain was meshed utilizing the snappyHexMesh tool available in OpenFOAM. Surrounding grids of the models were restructured, leading to the creation of high-quality surface mehes achieved with the application of six topoSets. Also, the value of the variable Y+ around the body was between 20 and 50 according to the Figure 4(e).

As mentioned before, In the CFD analysis of the current study, at the first the blockMesh is generated as an initial background mesh. Afterward toposets are applied according to the dimensions of the hull and domain in order to refinement of the initial background mesh and consequently new background mesh is

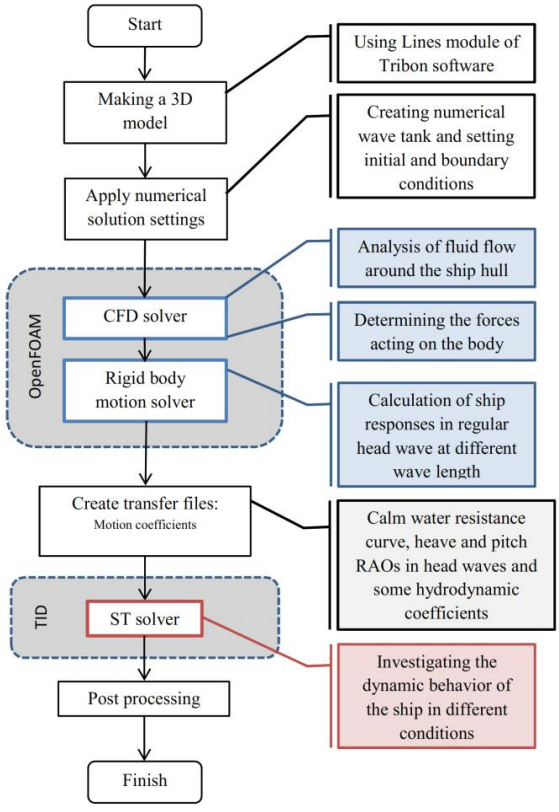

Figure 3. Hybrid solution flowchart of CFD-strip theory

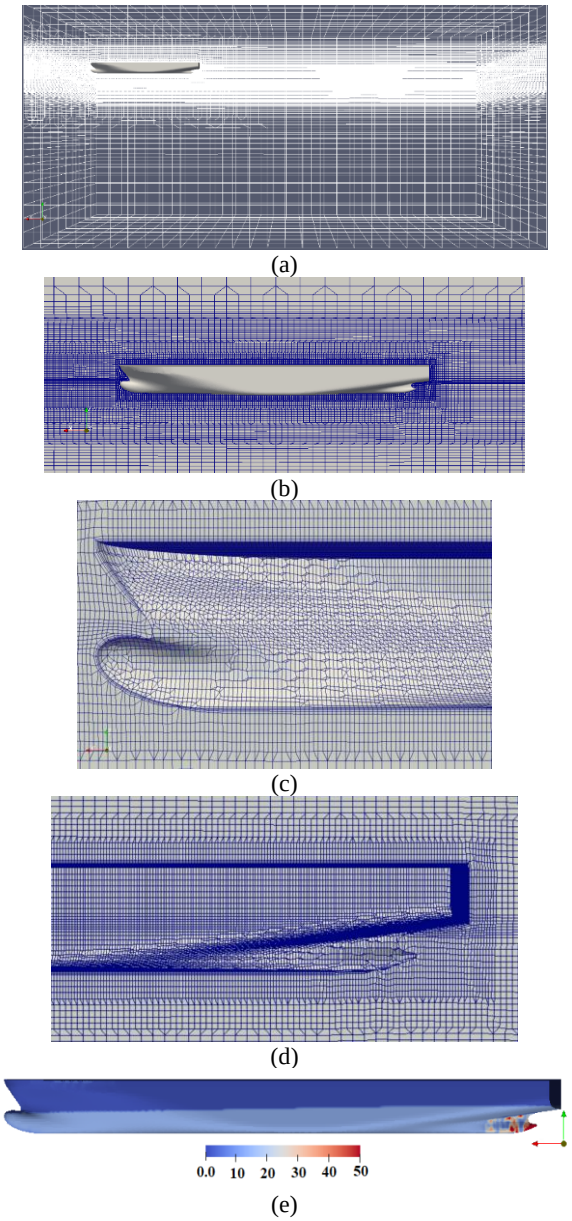

Figure 4. Mesh structure in the (a) main domain, (b) around the DTC hull, (c) fore, (d) aft areas and Y+ contour (e)

provided. Then the boundary layer mesh is generated around the ship hull. For mesh sensitivity analysis, there different grids with refinement ratio √2 are investigated as may be seen in Table 5.

Uncertainty analyses are considered based on the ITTC 2017. Details on the conducted methodology for deterministic uncertainty analysis are reo[ported in literature (44, 45). For mesh sensitivity analysis, calm water resistance at Fr=0.2, and heave and pitch RAOs under the Lw/Lm=1 are assessed compared to the experimental data as tabulated in Table 6. Based on the results presented in Table 6, for all three parameters of calm water resistance, heave RAO, and pitch RAO, an acceptable accordance is obtained between our results of Grid G2 (i.e., Medium) and experimental data. More details of validation study by selected mesh structure are presented for calm water and wavey condition in sections 3.1 and 3.2, respectively.

In the present study the maximum boundary layer thickness is about 5.1 cm and in the mesh structure 15 cells in the boundary layers are considered with growth rate of 1.3 to ensure the first cell centroid lies within the viscous sublayer in the SST k-ω turbulence model.

There is a fundamental challenge to the validation process. Research involving ship dynamic analysis has presented its results based on smaller scale models. Typically, the prototype undergoes dynamic analysis using the strip theory method. Since the heave and pitch RAO diagrams are dimensionless, analyzing and evaluating the dynamic results related to them is straightforward. On the contrary, the results obtained in the field of resistance are completely dependent on the scale of the ship. Therefore, the resistance in calm water and the added resistance in waves should be evaluated with other techniques. The validation section of this study has implemented a process to guarantee the accuracy of the results. The resistance of the ship has been obtained by different methods and based on different scales and compared with published data. The model scale has guided the evaluation of the ship's dynamic responses.

TABLE 5. Grids for mesh sensitivity analysis in CFD studies (refinement ratio $\sqrt{2}$)

Grids	Type	Dimensions		Total mesh
		Initial background mesh	Final background mesh	
G_1	Fine	85 × 16 × 115	189 × 33 × 134	992158
G_2	Medium	80 × 14 × 100	180 × 30 × 110	706000
G_3	Coarse	70 × 12 × 95	170 × 25 × 100	504800

TABLE 6. Mesh sensitivity analysis on calm water resistance at Fr=0.2, and heave and pitch RAOs at Lw/Lm=1

Grids	Type	Total mesh	Calm water resistance	
			Current study	Exp. (16)
G_1	Fine	992158	26.4	25.6
G_2	Medium	706000	26.5	25.6
G_3	Coarse	504800	27.9	25.6

Grids	heave RAO		pitch RAO	
	Current study	Exp. [7]	Current study	Exp. (7)
G_1	0.370	0.365	0.435	0.45
G_2	0.375	0.365	0.430	0.45
G_3	0.395	0.365	0.410	0.45

3. 1. Calm Water Figure 5 presents and compares the hydrodynamic resistance of a ship in calm water with published data for both model and full-scale scenarios. Figures 5(a) and 5(b), respectively, show the comparison of the resistance of the full-scale DTC hull, simulated using Holtrop and Mennen's method, and the model scale, simulated using FVM, with the published data (46). As may be seen in Figure 5, the CFD results of the current study (using FVM) are in high accordance with the published data. In this study, CFD results for resistance calculation are imported to Tribon software as an assumption for seakeeping simulation. With this, the calculation error related to the resistance in calm water has been minimized.

Table 7 shows the total resistance values for different Froude numbers, and the value obtained from the numerical solution of the present study can be compared with the experimental and numerical data of Moctar et al. (16).

3. 2. Dynamic Responses: Condition in Wave After ensuring the accuracy of the results in estimating the calm water resistance, the dynamic response and added resistance of the DTC hull are validated against the published experimental and numerical results (7, 46, 47).

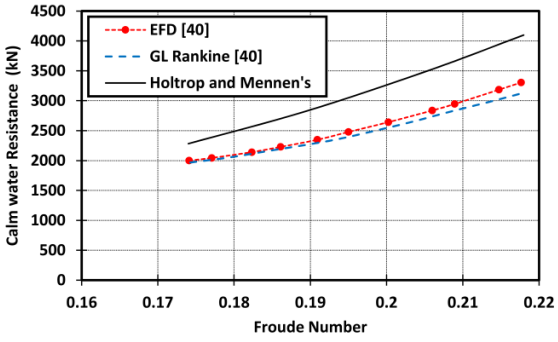

(a)

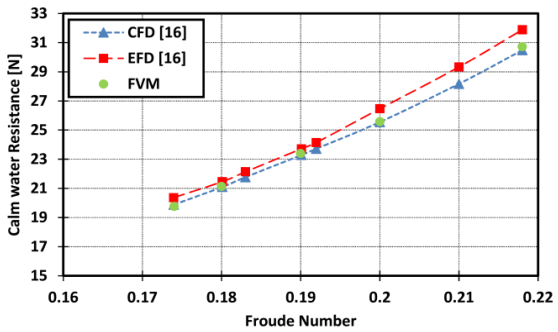

(b)

Figure 5. Hydrodynamic characteristics of (a) resistance of DTC ship (full scale), and (b) resistance of DTC ship (model)

TABLE 7. Comparison of the total resistance in calm water condition under different Froude numbers.

Froude Number	EFD (16)	Current Study	Error (%)	CFD (16)	Error (%)
0.174	20.330	19.767	2.773	19.740	2.905
0.180	21.491	21.142	1.624	21.008	2.248
0.190	23.784	23.408	1.581	23.220	2.371
0.200	26.506	25.647	3.241	25.486	3.849
0.218	32.002	30.767	3.859	30.499	4.698

Therefore, the heave and pitch RAOs and added resistance of the current study (both hybrid method and FVM) at Froude number (Fr) of 0.139 are compared to the published numerical and experimental data in Figure 6. As may be seen in Figure 6, good accordance is observable between our CFD results (using OpenFOAM code) with experimental data both in values and trend. However, the higher (but acceptable) mismatch is visible in our results using the hybrid method compared to the cited published works. Details of heave RAOs are also tabulated in Table 8.

It is worth mentioning that integrating the current hybrid approach with machine learning techniques (as may be seen in literature (48-55)) can constitute an additional strategy for achieving an approximately fast and accurate approach for predicting ship dynamics.

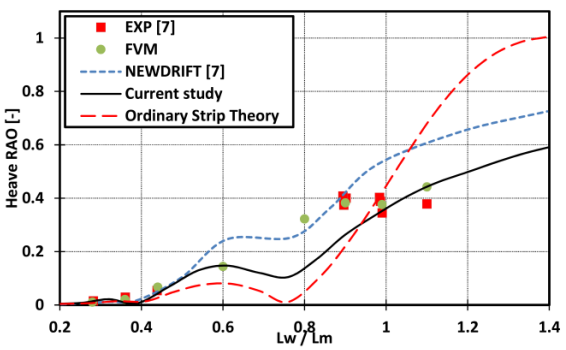

(a)

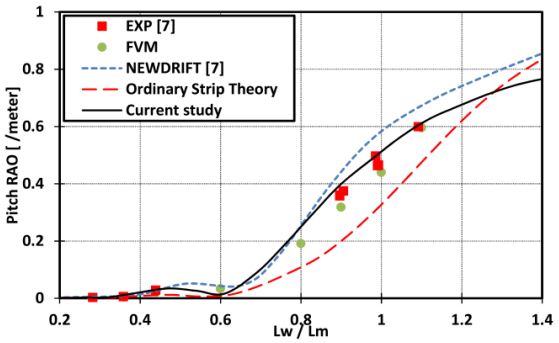

(b)

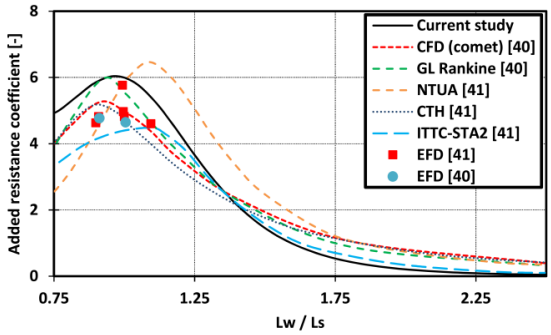

(c)

Figure 6. The comparison of current study (both of strip theory and FVM) with experimental and numerical data [7, 47, and 48] at Fr=0.139: (a) Heave RAO, (b) Pitch RAO, and (c) Added resistance

TABLE 8. Quantitative comparison on heave RAO values.

Lw/Ls	Exp. (7)	Current study	Error (%)	Ordinary Strip Theory	Error (%)
0.280	0.017	0.014	18.338	0.009	45.861
0.359	0.026	0.006	77.385	0.015	41.687
0.438	0.053	0.041	23.056	0.028	46.116
0.900	0.369	0.268	27.261	0.198	46.254
0.986	0.396	0.350	11.540	0.418	5.382
1.102	0.379	0.382	0.804	0.667	75.944

4. RESULTS AND DISCUSSION

In the current section, the dynamic responses and added resistance of DTC hull are studied using modified strip theory under various environmental and physical conditions. Usually, the dynamic analysis of a ship is more focused on its operational conditions. This means that the dynamic responses, such as heave and pitch

RAOs diagrams, are evaluated under normal loading conditions. While the ship at sea is facing conditions that may have a significant impact on its performance compared to the design point. These conditions include different load conditions on the one hand and the direction of incident waves on the other hand. The different conditions evaluated in this study are shown in Figure 7. Five drafts and six different trim angles are considered to simulate different loading conditions. Also, based on Figure 7, the angle of the incident wave and ship velocity vector is considered to be equal to 180 degrees in head wave conditions. In the dynamic analysis of floating in waves by the method presented in this study, there are two approaches: RAO diagrams, which are generally obtained based on the dynamic responses of the ship in different wavelengths, and RMS diagrams, which are presented for the analysis of the maximum of a parameter (for example, RAO).

4. 1. Effects of Ship Speed on Trim and Sinkage in Calm Water In this study, the effects of draft and trim on the dynamic behavior of the ship in waves have been investigated. Drafts and trim angles are selected based on the different loading conditions of the ship. Before studying the motions of the ship in different conditions, the amount of trim and sinkage of the ship should be investigated in the design loading condition at different speeds. In Figure 8, the trim and sinkage of the model can be seen at different Froude numbers in calm water. It is quite evident that the trim and sinkage of this hull form have very little change against the speed. So, due to the insignificant changes in trim and dynamic sinkage compared to the values caused by the loading condition, it is possible to skip applying the initial values for these two variables.

4. 2. Effects of Loading Condition (draft) in Different Wave Directions Typically, the design draft of a ship undergoes dynamic analysis. Changes in the ship's deadweight may cause the mission at sea to operate under conditions that differ from the ship's design scenario. One of the conditions evaluated here is the dynamic behavior of the ship in different drafts. Also, ship motions during its operation are significantly dependent on the wave direction. Moreover, the wave propagation angle determines the frequency of the wave encountering the ship and has a significant effect on its added resistance at different ship speeds. Based on this, five different drafts (10, 12, 14.5, 17, and 19 m) have been selected to investigate the ship motions. Figures 9 and 10 show the heave and pitch RAOs at different drafts under various wave directions, respectively. In addition, the effects of wave direction ranging from 180° to 90° on heave and pitch RAOs and added resistance are investigated.

As may be seen in Figure 9, three main regions are evident in the diagram, including the interval of low Lw/Ls (i.e., Lw/Ls: 0.2≈ 0.7), the interval of medium Lw/Ls (i.e., Lw/Ls: 0.7≈ 1.1), and the interval of high Lw/Ls (i.e., Lw/Ls upper than 1.1). In the case of low Lw/Ls, the effects of the change in the draft on the heave RAO are negligible. For medium Lw/Ls, increasing the draft results in a lower heave RAO. For high Lw/Ls, a greater draft results in a higher heave RAO. Reducing the angle of the incident wave results in a reduction in the

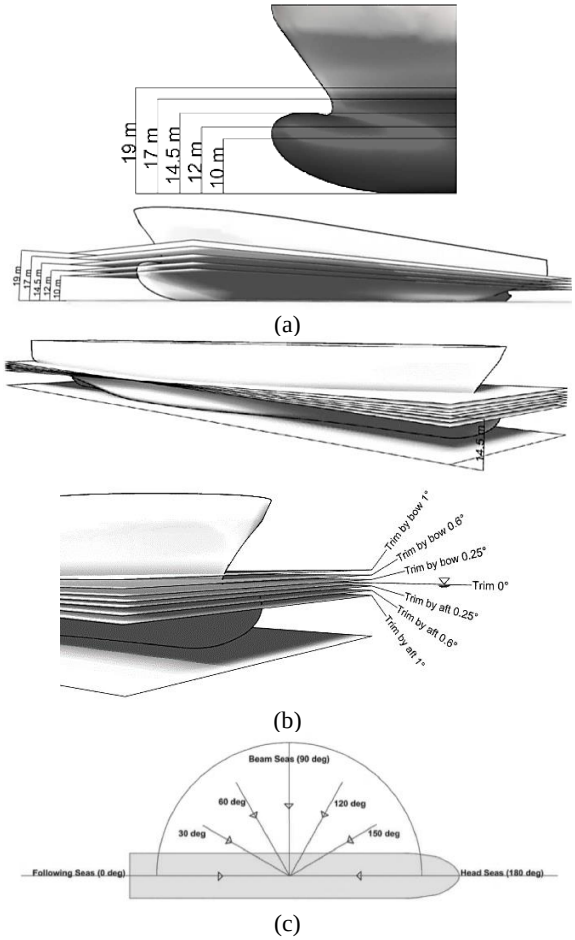

Figure 7. The definition of DTC hull at different: (a) draft, (b) trim and (c) wave direction

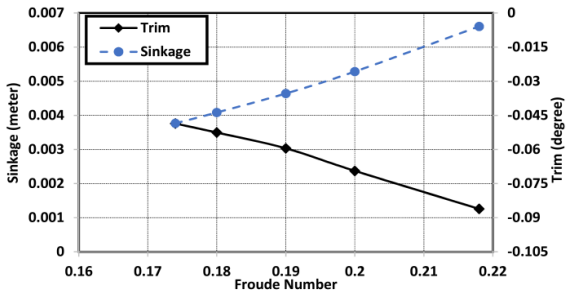

Figure 8. Trim and sinkage changes in calm water for different Froude Numbers

range of the mentioned intervals. Figure 10 shows that a reduction in draft leads to a higher pitch RAO for all wave directions. Moreover, a change in the draft from 12 to 14.5 (the design draft of the full-scale DTC hull) significantly increases the rate of pitch RAO changes.

Also, the higher heave RAO is achieved for a wave direction of 90°. Moreover, by decreasing the wave angle from 180° to 90°, the heave RAO has a more significant gradient and converges faster to a limit value. This is because changing the wave angle from 180° to 90° causes the heave motion amplitude to converge with the wave amplitude, thereby reducing interference effects. Figure 10 illustrates that greater wave angles also result in higher pitch RAO. Furthermore, reducing the wave angle from 150° to 120° significantly increases the pitch RAO reduction compared to reducing the wave angle from 180° to 150°. The effective wavelength is directly affected by alterations in the angle of the wave's encounter. Likewise, the dynamics of heave and pitch are subject to the effects of wavelength. In this regard, more explanations are provided in the polar diagrams section.

The effects of different drafts on the added resistance of the DTC hull under various wave angles are studied and presented in Figure 11. Figure 11 shows that when the Lw/Ls ratio is less than 1, a lower draft leads to a higher added resistance, with the added resistance

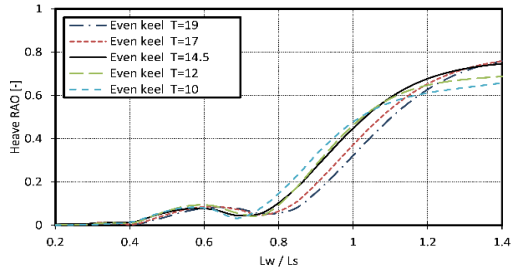

(a) 180°

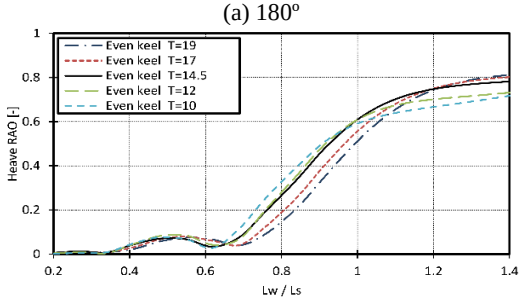

(b) 150°

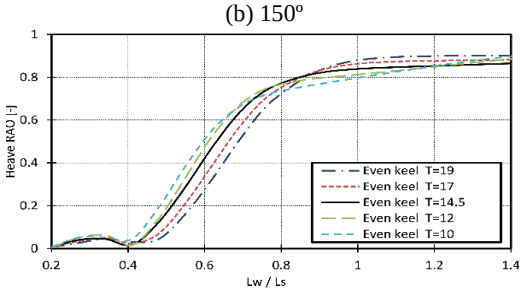

(c) 120°

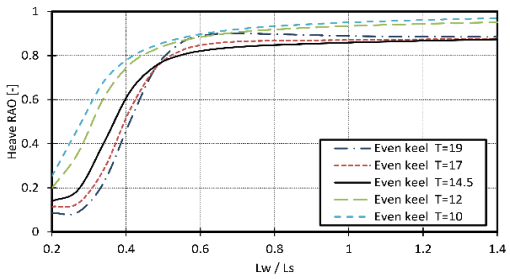

(d) 90°

Figure 9. Heave RAOs at different drafts under various wave directions of (a) 180°, (b) 150°, (c) 120°, and (d) 90° (at Fr=0.218)

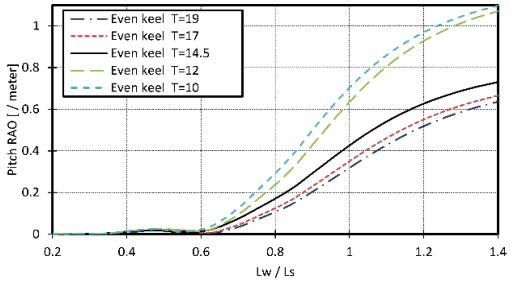

(a) 180°

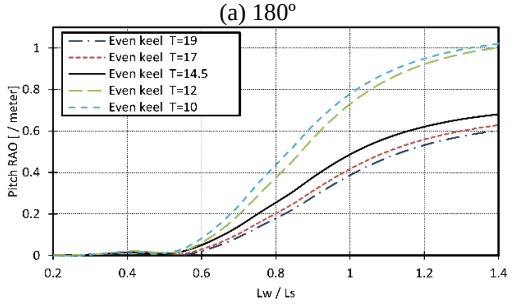

(b) 150°

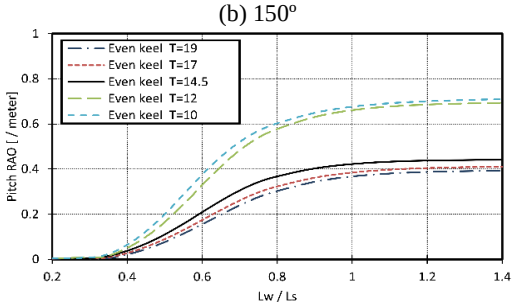

(c) 120°

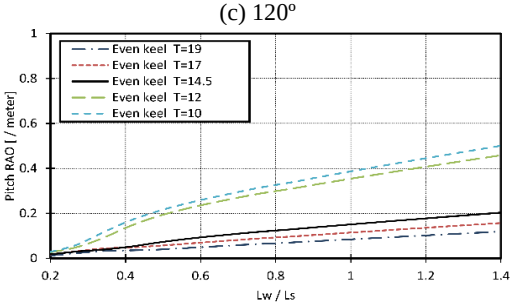

(d) 90°

Figure 10. Pitch RAOs at different drafts under various wave directions of (a) 180°, (b) 150°, (c) 120°, and (d) 90° (at Fr=0.218)

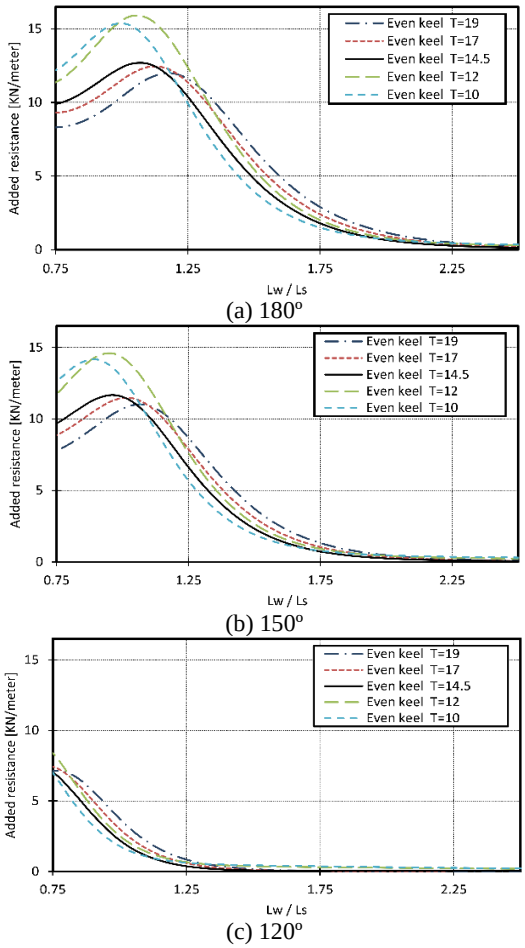

Figure 11. Added resistance at different drafts under various wave directions of (a) 180°, (b) 150°, and (c) 120° (at Fr=0.218)

peaking at T= 12 m at Lw/Ls = 1. Moreover, for Lw/Ls > 1.9, the effect of changing the draft on the added resistance is negligible. Furthermore, reducing the angle of wave direction increases the maximum value of the added resistance. Moreover, the maximum added resistance for drafts of 10 and 12 m is significantly different compared to other drafts. Based on Figure 11, higher added resistance occurs by increasing the wave angle from 120° to 180°. Additionally, increasing the wave angle shifts the peak of the added resistance from a lower wavelength to a higher one.

4. 3. Effects of Trim angle under Different Wave Directions The trim angle of a ship is another impressive factor in its dynamic response. Because the changes in the loading condition of the ship can lead to the displacement of its center of gravity and consequently the trim of the ship. Therefore, in this subsection, the effects of three different trim angles of 0.25, 0.6, and 1 degree (both for trim by aft and trim by bow) on the dynamic responses and added resistance of the DTC hull are investigated. Figures 12 and 13 show the heave and pitch RAOs at different trim angles under various wave directions, respectively. Figure 12 shows that when the ship is in a 1° trim by aft, the maximum heave RAO occurs at a wave angle of 120°. Figure 12(a) demonstrates that an increase in the trim angle towards the ship's stern (trim by aft) increases the heave RAO in the greater wavelength (Lw/Ls>1). We record the minimum value when we apply the same trim angle towards the ship's bow (trim by bow). Additionally, the maximum heave RAO value was observed at angles toward the ship's bow, specifically at an incident wave angle of 90°. An increase in wave angles up to 180° reverses this trend. Figure 13 illustrates that an increase in trim by the bow enhances pitch RAO, while a greater angle of trim by the aft results in lower pitch RAO. Moreover, a smoother gradient of pitch RAO is observed at a greater angle of trim by aft. All tested angles of the wave direction also exhibit this behavior. In the heave RAO diagram, when the wave angle shifts from 180 to 90 degrees (head wave to beam wave), the dynamic response range for the even keel condition under long waves broadens in comparison to other trim conditions. The pitch RAO diagram does not show such a trend.

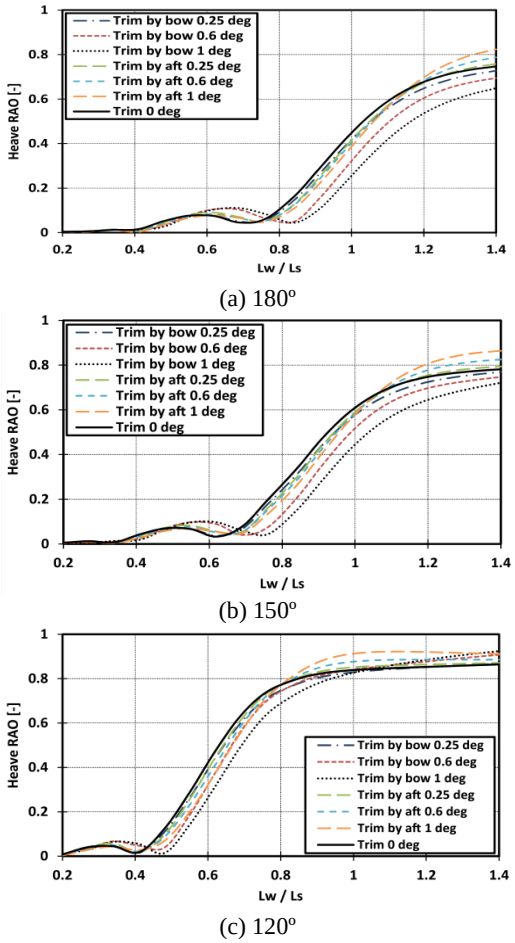

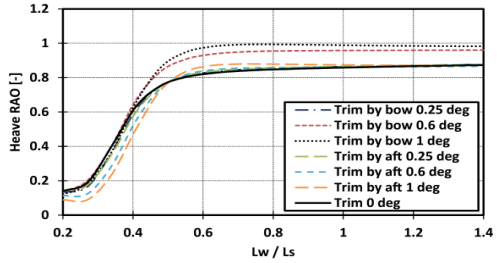

(d) 90º

Figure 12. Heave RAO at different trim angles under various wave directions of (a) 180°, (b) 150°, (c) 120°, and (d) 90° (at Fr=0.218)

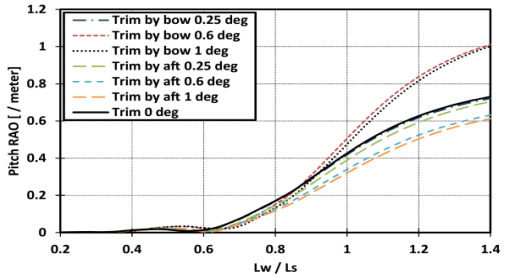

(a) 180º

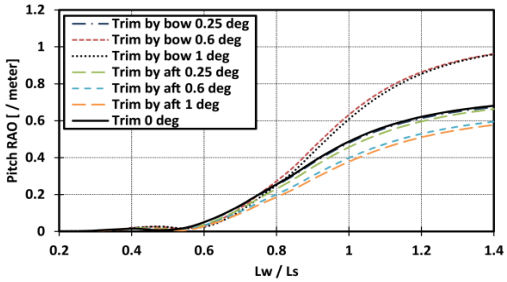

(b) 150º

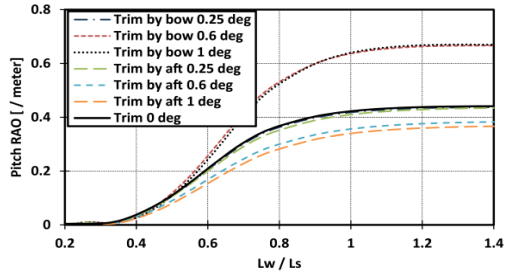

(c) 120º

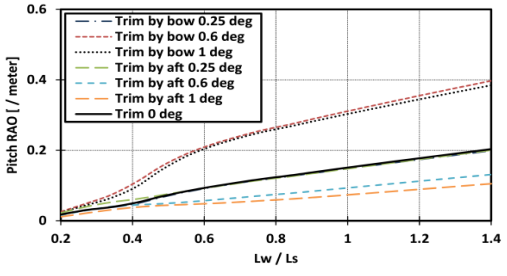

(d) 90º

Figure 13. Pitch RAO at different trim angles under various wave directions of (a) 180°, (b) 150, (c) 120°, and (d) 90° (at Fr=0.218)

Figure 14 investigates the effects of different trim angles on the DTC hull's added resistance under various incident wave angles. Figure 14 shows that trim by aft reduces the added resistance of the DTC hull. The maximum added resistance is visible when the trim angle is equal to 1°. Moreover, changes in added resistance are more common when the trim angle is higher than 0.6, while the results of added resistance for other trim angles are closer together. For wave angles of 150 degrees and 180 degrees, waves with a short length add even less resistance (Lw/Ls >1) than when the trim is by aft, which is called an "even keel condition." Meanwhile, even keel conditions yield the lowest value of added resistance for longer wavelengths.

4. 4. Effects of Speed and Wave Direction Polar diagrams are usually used to simultaneously analyze the effects of ship speed and wave direction. Polar diagrams can also cover a wider range of wave angles. Figure 15 presents the heave, pitch, and added resistance polar

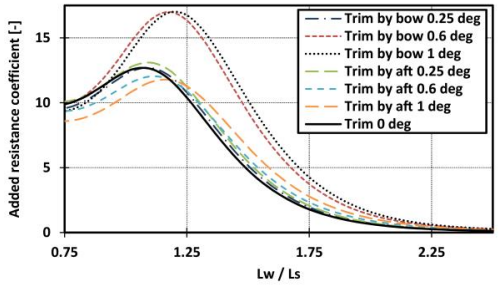

(a) 180º

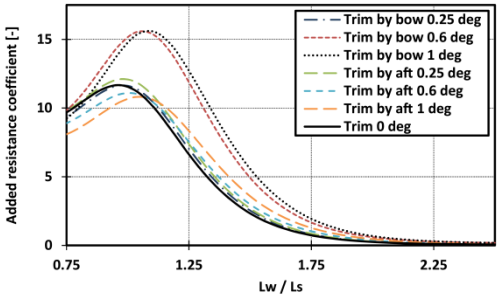

(b) 150º

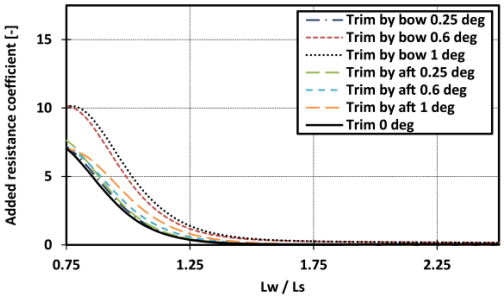

(c) 120º

Figure 14. Added resistance at different trim angles under various wave directions of (a) 180°, (b) 150°, and (c) 120° (at Fr=0.218)

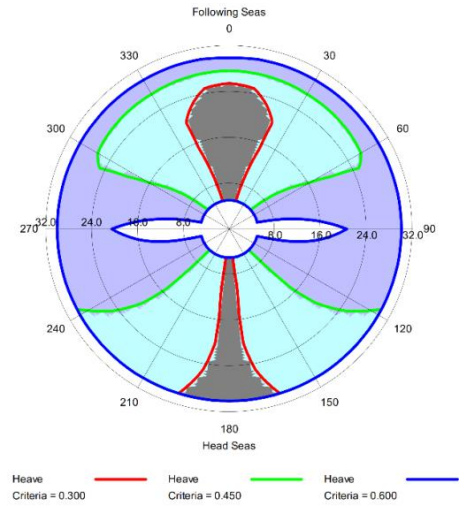

(a) RMS heave

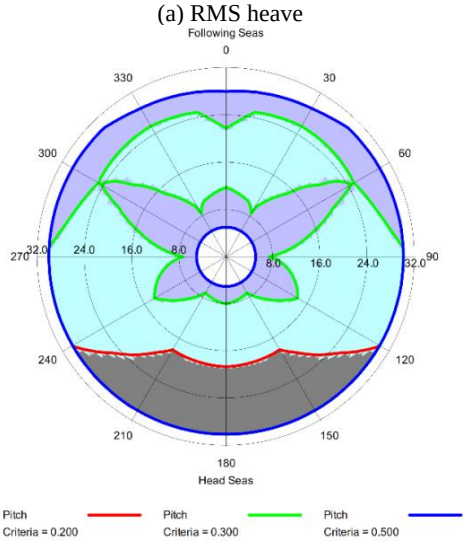

(b) RMS pitch

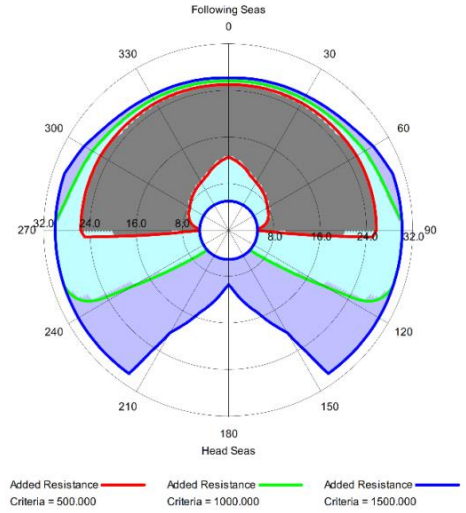

(c) RMS added resistance

Figure 15. RMS of heave (a) RMS pitch (b) RMS added resistance (c) of the ship at DWL according to the incident wave angles

diagrams to provide a more accurate understanding of the effects of wave direction at different ship speeds. For each of the graphs, three criteria were determined based on the maximum and minimum RMS values. The blue (0.6), green (0.45), and red (0.3) curves in Figure 15(a) represent the selected criteria for heave motion. The regions between these curves are also displayed in such a way that they can be distinguished from each other. For example, the gray region represents the points where the heave RAO values are less than 0.3. This indicates that under head and following wave conditions, the heave RAO values are less than 0.3. The situation remains the same for pitch RAO. Figure 15(c) shows that the head wave condition yields the maximum values for the added resistance. This means that in the case where the angle of the waves is 180 degrees, the amount of added resistance for speeds higher than 10 knots can also exceed the maximum criterion. It should be noted that the graphs presented in Figure 15 were obtained in the design draft and trim condition. Also, the added resistance is presented here in its initial form and based on the Newton units.

For both the heave and pitch motions, the lowest RMS value was recorded in the head seas condition. The reason for this is that in this case the ratio of encountered wavelength to ship length is at its lowest value. In contrast, the highest added resistance value was recorded in the head seas condition. the combination of direct wave impact, increased energy dissipation, pitching and heaving motions, wave breaking, and hydrodynamic forces all contribute to the maximum added resistance experienced by a ship in head wave conditions.

4. 5. Phenomenological Study The present study has obtained many hydrodynamic parameters of the ship using a numerical method. One of the most important parameters is resistance, trim, and sinkage in calm water at different speeds. Also, the dynamic analysis of the ship in the regular wave under head wave conditions is done by numerical method. It is necessary to describe some hydrodynamic and dynamic phenomena in the ship using the contours presented in this section. Figures 16 and 17, respectively, show the changes in the free surfaces from the top and side views in calm water. As may be seen in Figures 16 and 17, the height of the generated wave by the DTC hull is increased by an enhancement in ship speed, especially at the ship's stern. The draft of the ship in calm water is equal to 0.244 m. Therefore, the maximum and minimum values of the free surface elevations in Figures 16 and 17 are set so that the fluctuations of the free surface can be observed in relation to the mean waterline. In Figure 16, it can be seen that with the increase in the Froude number, the effect of the waves produced by the hull in the two areas of the fore and aft expands more in the y direction.

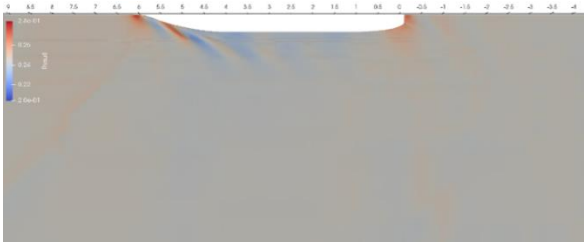

(a) Fr=0.174

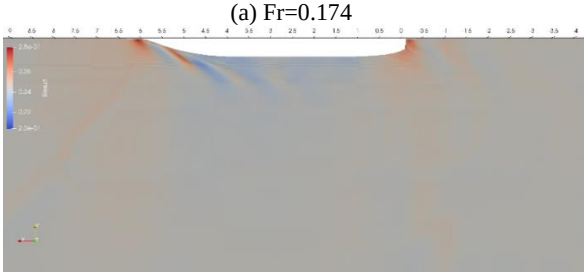

(b) Fr=0.18

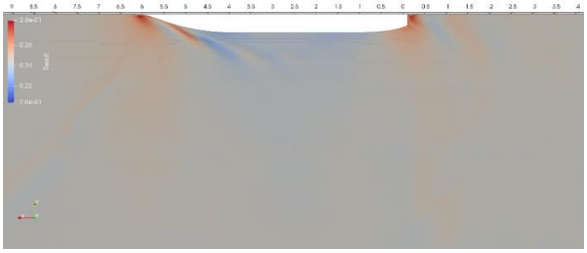

(c) Fr=0.19

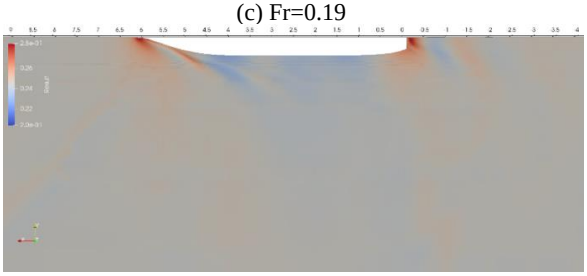

(d) Fr=0.2

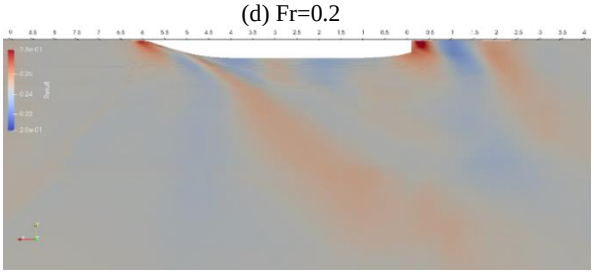

(e) Fr=0.218

Figure 16. The free surface elevation around the DTC hull from the top view in calm water (t=20 s) at different Froude numbers

Figures 18 and 19 show the changes in the free surface from the top and side views in wave conditions. All contours are recorded at t = 20s and design speed to be able to make a more accurate comparison between the water levels in different conditions. Significant changes in the height of the free surface can be related to the heave RAO value at Lw/Ls=1.1.

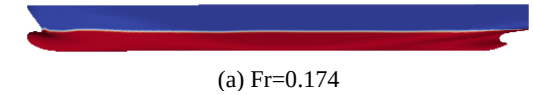

(a) Fr=0.174

(b) Fr=0.18

(c) Fr=0.19

(d) Fr=0.2

(e) Fr=0.218

Figure 17. Contours α=0.5 from the side view of the DTC hull in calm water (t=20s) at different Froude numbers

Free surface contour analysis is important because it indicates the height of the waves around the ship's hull. On the other hand, the energy carried by a wave is directly proportional to the square of its amplitude. Therefore, by analyzing the height (amplitude) of the waves, it is possible to obtain their energy changes along the length of the ship. Any change in this energy indicates the amount of energy that the ship and the seawater have exchanged. One of the remarkable points in Figures 18 and 19 are the great effects of the presence of the hull on the range of changes of the free surface around it. One of the assumptions of using the strip theory method is that the presence of a hull does not affect the waves in the x direction.

Figure 20 illustrates the fluctuations of the free surface at various points as a function of the design speed

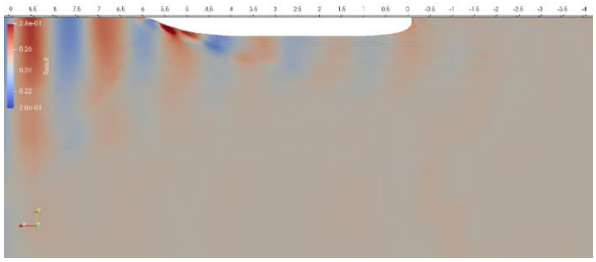

(a) L_w/L_s =0.28

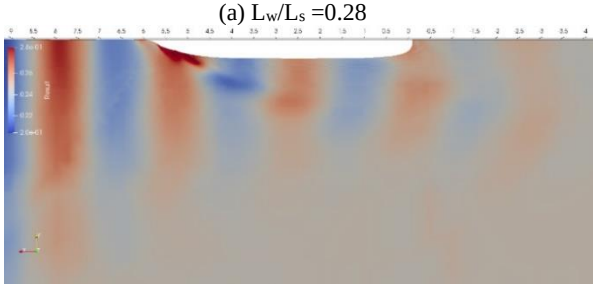

(b) L_w/L_s =0.44

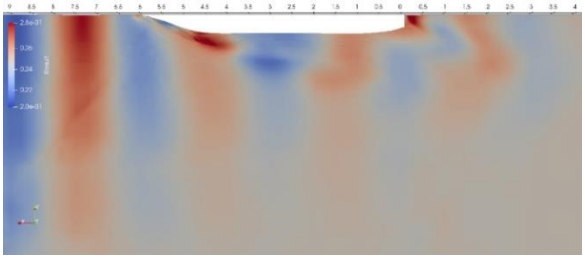

(c) L_w/L_s =0.5

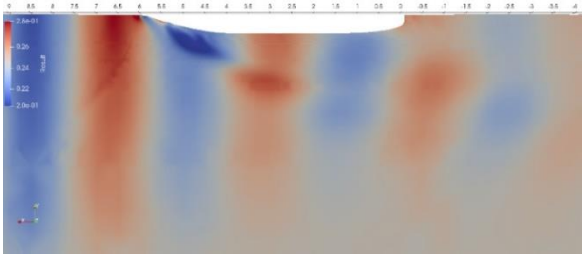

(d) L_w/L_s =0.6

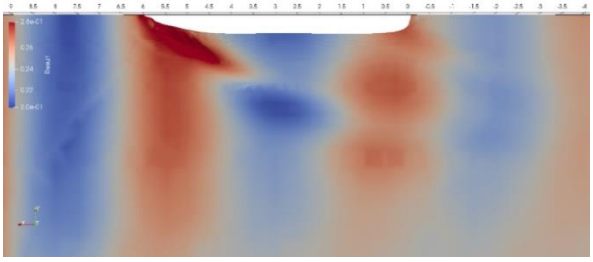

(e) L_w/L_s =0.8

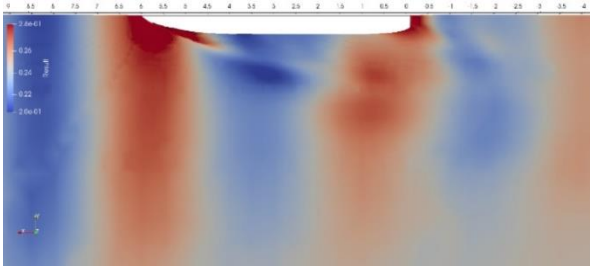

(f) L_w/L_s =0.83

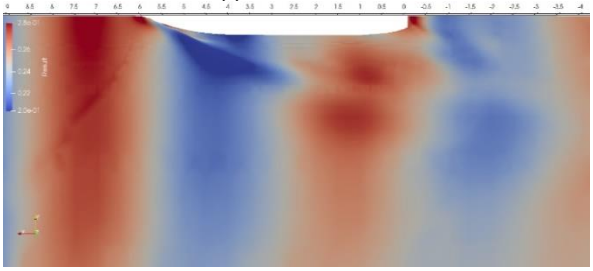

(g) L_w/L_s =1

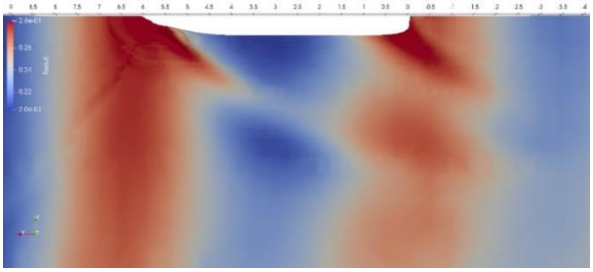

(h) L_w/L_s =1.1

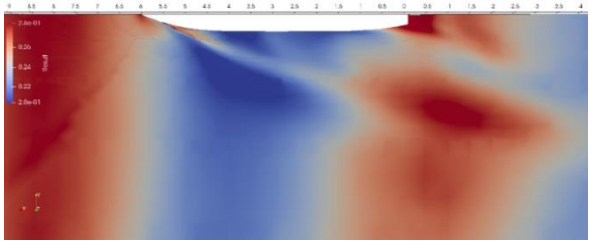

(i) L_w/L_s =1.5

Figure 18. The free surface elevation around the DTC hull from the top view at condition in wave (t=20 s) under various wave lengths

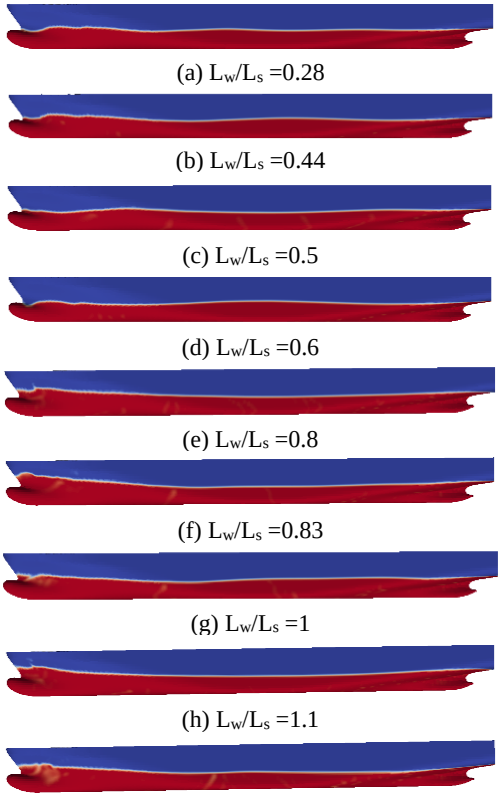

(a) L_w/L_s =0.28

(b) L_w/L_s =0.44

(c) L_w/L_s =0.5

(d) L_w/L_s =0.6

(e) L_w/L_s =0.8

(f) L_w/L_s =0.83

(g) L_w/L_s =1

(h) L_w/L_s =1.1

(i) L_w/L_s =1.5

Figure 19. Contours α=0.5 from the side view of the DTC hull at condition in wave (t=20 s) under various wave lengths

versus time. The position of 4 points is shown in Figure 20(a). Point 1 is chosen in such a way that the fluctuations of the free surface are not affected by the shape of the body. The free surface oscillation amplitude here is equal to the input wave amplitude. Point 2 is located at the place where the largest number of changes or fluctuations of the free surface was recorded at t = 20s. In Figure 20(b), the examination of water level fluctuations against time at point 2 shows that the positive and negative range of the free surface is also greater at this point than at other points. Points 3 and 4 also exhibit this trend, albeit with a smaller range. The average bandwidths at every point are also observable in Figure 20(b).

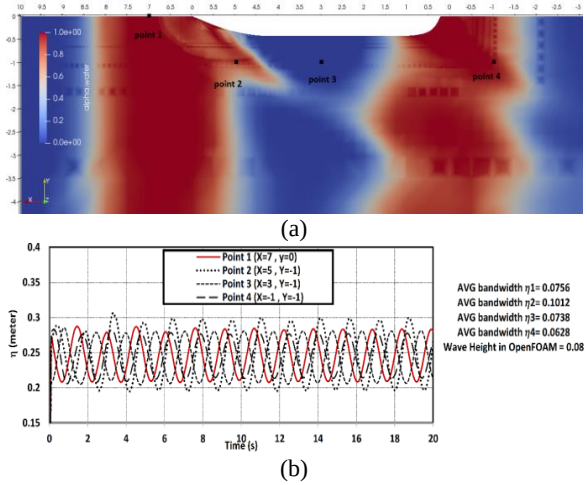

(a)

(b)

Figure 20. Illustration of (a) position of different point around the DTC hull at t=20 s and Lw/Ls=1.1, and (b) free surface elevations at different positions around the hull

5. CONCLUSION

This paper numerically investigates the added resistance and seakeeping of the DTC hull under various geometrical and environmental conditions. For this purpose, five different DTC hull drafts in the range of 10 m to 19 m and three trim angles ranging from 0.25° up to 1° are considered under various incident wave angles from 90° to 180°. In addition, the CFD-strip theory hybrid method is also used for numerical simulation. In the current methodology, the RANS method using the FVM scheme is implemented with the open-source software OpenFOAM, while the strip theory method is conducted by Tribon. Based on this method, the ship's dynamic motions in regular head waves have been analyzed by using the computational fluid dynamics method. Because the results of the numerical method are more accurate than the strip theory method compared to the experimental data. Then, the hydrodynamic coefficients of the ship obtained by the numerical method are used as the input of the strip theory method. With this technique, more accurate results are obtained in a shorter time using the strip theory method. To ensure the accuracy of the considered methodology, the present study results are compared with published experimental and numerical data, and acceptable accordance is achieved. The major extracted findings from the current study are as follows:

a. An increase in incident wave angles enhances the slope of the heave RAO diagram. Furthermore, a smaller incident wave angle results in a lower pitch RAO. The rate of difference in the heave and pitch RAOs is more pronounced when the incident wave angle varies from 120° to 150°, compared to other cases. Increasing the incident wave angles from 120° to 180° also enhances the added resistance.
b. Non-uniform changes in the heave RAO due to draft changes are observed. The effects of draft changes are negligible at small wavelengths, while an increase in draft at medium and large wavelengths results in lower heave RAO and higher RAO, respectively. Moreover, draft reduction causes a higher pitch for RAO. The maximum of added resistance is also achieved for T = 12 m in the case of a wavelength equal to the length of the DTC hull.
c. For an incident wave angle of 120°, the heave RAO reaches its maximum at 1° trim by aft. At a small wavelength, an increase in aft trim results in a higher heave RAO. Moreover, an enhancement in trim by the bow increases pitch RAO. We also achieve the maximum added resistance when trim by bow equals 1°.
d. For wave angles of 150 degrees and 180 degrees, waves with a short length add even less resistance (Lw/Ls>1) than when the trim is by aft, which is called an "even keel condition." Meanwhile, even keel conditions yield the lowest value of added resistance for longer wavelengths.

Finally, one can conclude that using a CFD-strip theory hybrid model can be considered fast, inexpensive, and sufficiently accurate for practical applications in investigating the added resistance and seakeeping of merchant ships.

However, the ship dynamics analysis in this study was performed based on 6 degrees of freedom, the present investigation has limitations from the point of view of presenting only the heave and pitch RAOs of the DTC hull under various trims and drafts. Therefore, the current study warrants further investigation, including examining the vertical accelerations at the vessel's bow, bridge, and stern, exploring the hybrid method of combining other CFD solvers with OpenFOAM, and considering alternative standard merchant hull forms. It should be noted that in the current study, the accuracy of the simulation was investigated on a commercial displacement vessel. Therefore, the use of this method for planing hulls and high speeds requires further analysis.

6. REFERENCES

1. List T. International Towing Tank Conference. 2011.
2. Moctar Oe, Shigunov V, Zorn T. Duisburg Test Case: Post-panamax container ship for benchmarking. Ship Technology Research. 2012;59(3):50-64. https://doi.org/10.1179/str.2012.59.3.004
3. Park D-M, Lee J, Kim Y. Uncertainty analysis for added resistance experiment of KVLCC2 ship. Ocean Engineering. 2015;95:143-56. https://doi.org/10.1016/j.oceaneng.2014.12.007
4. Park D-M, Kim Y, Seo M-G, Lee J. Study on added resistance of a tanker in head waves at different drafts. Ocean Engineering. 2016;111:569-81. https://doi.org/10.1016/j.oceaneng.2015.11.026

5. Sprenger F, Hassani V, Maron A, Delefortrie G, Van Zwijnsvoorde T, Cura-Hochbaum A, et al., editors. Establishment of a validation and benchmark database for the assessment of ship operation in adverse conditions. International Conference on Offshore Mechanics and Arctic Engineering; 2016: American Society of Mechanical Engineers.
6. Park D-M, Lee J-H, Jung Y-W, Lee J, Kim Y, Gerhardt F. Experimental and numerical studies on added resistance of ship in oblique sea conditions. Ocean Engineering. 2019;186:106070. https://doi.org/10.1016/j.oceaneng.2019.05.052
7. Liu S, Sprenger F, Papanikolaou A, Dafermos G, Zaraphonitis G. Experimental and numerical studies on linear and nonlinear seakeeping phenomena of the DTC ship in regular waves. Ship Technology Research. 2021;68(1):41-61. https://doi.org/10.1080/09377255.2020.1857007
8. Kinaci OK, Gokce MK, Delen C. Resistance experiments and self-propulsion estimations of Duisburg Test Case at 1/100 scale. Ship Technology Research. 2020;67(2):109-20. https://doi.org/10.1080/09377255.2020.1729454
9. Lee J-H, Kim Y, Kim B-S, Gerhardt F. Comparative study on analysis methods for added resistance of four ships in head and oblique waves. Ocean Engineering. 2021;236:109552. https://doi.org/10.1016/j.oceaneng.2021.109552
10. Chirosca A-M, Medina A, Pacuraru F, Saettone S, Rusu L, Pacuraru S. Experimental and numerical investigation of the added resistance in regular head waves for the DTC hull. Journal of Marine Science and Engineering. 2023;11(4):852. https://doi.org/10.3390/jmse11040852
11. Guo B, Steen S, Deng G. Seakeeping prediction of KVLCC2 in head waves with RANS. Applied Ocean Research. 2012;35:56-67. https://doi.org/10.1016/j.apor.2011.12.003
12. Sadat-Hosseini H, Wu P-C, Carrica PM, Kim H, Toda Y, Stern F. CFD verification and validation of added resistance and motions of KVLCC2 with fixed and free surge in short and long head waves. Ocean Engineering. 2013;59:240-73. https://doi.org/10.1016/j.oceaneng.2012.12.016
13. Gasparotti C, Rusu L. Seakeeping performance assessment for a containership in a specific sea area. Mechanical Testing and Diagnosis. 2013;3(1):38-48.
14. Liu S, Papanikolaou A, editors. Prediction of the added resistance of ships in oblique seas. ISOPE International Ocean and Polar Engineering Conference; 2016: ISOPE.
15. Islam H, Akimoto H, editors. Prediction of ship resistance in Head Waves Using RaNS based solver. AIP Conference Proceedings; 2016: AIP Publishing.
16. Moctar Oe, Sigmund S, Ley J, Schellin TE. Numerical and experimental analysis of added resistance of ships in waves. Journal of Offshore Mechanics and Arctic Engineering. 2017;139(1):011301. https://doi.org/10.1115/1.4034205
17. Papanikolaou A, Fournarakis N, Chroni D, Liu S, Plessas T, Sprenger F, editors. Simulation of the maneuvering behavior of ships in adverse weather conditions. Proceedings; 2016.
18. He R, Zhang Z, Wang X, Feng D, editors. Numerical simulation of the ship bottom interaction of DTC container carrier for different keel clearance in pure sway motion. Proceedings of the 4th International Conference on Ship Manoeuvering in Shallow and Confined Water (MASHCON): Ship-Bottom interaction, Hamburg, Germany; 2016.
19. Liu C, Wang J, Wan D, Yu X, editors. Computation of Wave Drift Forces and Motions of DTC Ship in Oblique Waves. ISOPE International Ocean and Polar Engineering Conference; 2017: ISOPE.
20. Liu C, Wang J, Wan D. CFD computation of wave forces and motions of DTC ship in oblique waves. International journal of offshore and polar engineering. 2018;28(02):154-63. https://doi.org/10.17736/ijope.2018.sh21
21. Liu C, Chen G, Wan D, editors. CFD Study of Added Resistance and Motion of DTC in Short and Long Waves. International Conference on Offshore Mechanics and Arctic Engineering; 2018: American Society of Mechanical Engineers.
22. Srivastava A, Akhtar H, Gupta A, Kumar R. Hydrodynamic Analysis of the Ship Hull. Int J Emerg Technol Eng Res. 2019;4:25-8.
23. Islam H, Soares CG. Uncertainty analysis in ship resistance prediction using OpenFOAM. Ocean Engineering. 2019;191:105805. https://doi.org/10.1016/j.oceaneng.2019.02.033
24. Martic I, Chillcce G, Tello Ruiz M, Ramirez J, Degiuli N, Ould el Moctar B, editors. Numerical assessment of added resistance in waves of the DTC container ship in finite water depths. 5th Mashcon; 2019: Knowledge centre for manoeuvring in shallow and confined water.
25. Deng G, Guilmineau E, Leroyer A, Queutey P, Visonneau M, Wackers J, editors. Simulation of container ship in shallow water at model scale and full scale. Third Chinese National CFD Symposium on Ship and Offshore Engineering; 2014.
26. Chirosca A, Gasparotti C. Comparison between model test and numerical simulations for a container ship. Maritime Technology and Engineering 5 Volume 2: CRC Press; 2021. p. 75-80.
27. Amini-Afshar M. Salvesen's method for added resistance revisited. Journal of Offshore Mechanics and Arctic Engineering. 2021;143(5):051902. https://doi.org/10.1115/1.4050213
28. Kobayashi H, Kume K, Orihara H, Ikebuchi T, Aoki I, Yoshida R, et al. Parametric study of added resistance and ship motion in head waves through RANS: Calculation guideline. Applied Ocean Research. 2021;110:102573. https://doi.org/10.1016/j.apor.2021.102573
29. Mikkelsen H, Shao Y, Walther JHH, editors. CFD verification and validation of added resistance and seakeeping response in regular oblique waves with varying wave length: Paper 176. The 9th Conference on Computational Methods in Marine Engineering (Marine 2021); 2022.
30. Kinaci OK, Ozturk D. Straight-ahead self-propulsion and turning maneuvers of DTC container ship with direct CFD simulations. Ocean Engineering. 2022;244:110381. https://doi.org/10.1016/j.oceaneng.2021.110381
31. Fang X, Yu J, Yao C, Zhang Z, Wang X, editors. Numerical study on wave-induced drift forces and motions of a DTC ship in head and oblique waves using functional decomposition model. IOP Conference Series: Materials Science and Engineering; 2023: IOP Publishing.
32. Chowdhury JI, Faieq A, Amin OM. Seakeeping analysis of a tanker with hard sail-based wind propulsion system in various seaways. Ocean Engineering. 2023;278:114481. https://doi.org/10.1016/j.oceaneng.2023.114481
33. Liu S, Shang B, Papanikolaou A, Bolbot V. Improved formula for estimating added resistance of ships in engineering applications. Journal of Marine Science and Application. 2016;15:442-51. https://doi.org/10.1007/s11804-016-1377-3
34. Liu S, Papanikolaou A. On the prediction of the added resistance of large ships in representative seaways. Ships and Offshore Structures. 2017;12(5):690-6. https://doi.org/10.1080/17445302.2016.1200452
35. Islam H, Ventura M, Soares CG, Tadros M, Abdelwahab H. Comparison between empirical and CFD based methods for ship resistance and power prediction. Trends in maritime technology and engineering. 2022:347-57.
36. Lee J-H, Kim B-S, Kim Y. Study on steady flow effects in numerical computation of added resistance of ship in waves. Journal of Advanced Research in Ocean Engineering. 2017;3(4):193-203. https://doi.org/10.5574/JAROE.2017.3.4.193

37. Amini-Afshar M, Bingham HB. Added resistance using Salvesen–Tuck–Faltinsen strip theory and the Kochin function. Applied Ocean Research. 2021;106:102481. https://doi.org/10.1016/j.apor.2020.102481
38. Song X, Zhang X, Beck RF. Numerical study on added resistance of ships based on time-domain desingularized-Rankine panel method. Ocean Engineering. 2022;248:110713. https://doi.org/10.1016/j.oceaneng.2022.110713
39. Kashiwagi M. Numerical seakeeping calculations based on slender ship theory. Schiffstechnik. 1997;44(4):167-92.
40. Menter FR. Two-equation eddy-viscosity turbulence models for engineering applications. AIAA journal. 1994;32(8):1598-605. https://doi.org/10.2514/3.12149
41. Larsson L, Stern F, Visonneau M, editors. Numerical ship hydrodynamics. An assessment of the Gothenburg 2010 Workshop; 2014: Springer.
42. ITTC R. procedures and guidelines: practical guidelines for ship CFD applications, 7.5. ITTC: Boulder, CO, USA. 2011.
43. Stern F, Guilmineau E, Visonneau M, Toxopeus S, Simonsen C, Aram S, et al. CFD Validation for Surface Combatant 5415 at Straight-Ahead and 20 Degree Static Drift Conditions: NATO RTO/AVT-183, Technical Report; 2015.
44. Mousaviraad SM, He W, Diez M, Stern F. Framework for convergence and validation of stochastic uncertainty quantification and relationship to deterministic verification and validation. International Journal for Uncertainty Quantification. 2013;3(5). 10.1615/Int.J.UncertaintyQuantification.2012003594
45. Diez M, He W, Campana EF, Stern F. Uncertainty quantification of Delft catamaran resistance, sinkage and trim for variable Froude number and geometry using metamodels, quadrature and Karhunen–Loève expansion. Journal of Marine Science and Technology. 2014;19:143-69. https://doi.org/10.1007/s00773-013-0235-0
46. Lang X, Mao W. A semi-empirical model for ship speed loss prediction at head sea and its validation by full-scale measurements. Ocean Engineering. 2020;209:107494. https://doi.org/10.1016/j.oceaneng.2020.107494
47. TIN YADANAR T. Ship Hull Optimization in Calm Water and Moderate Sea States. 2016.
48. Taghva HR, Ghassemi H, Nowruzi H. Seakeeping performance estimation of the container ship under irregular wave condition using artificial neural network. Am J Civil Eng Archit. 2018;6(4):147-53. https://doi.org/10.12691/ajcea-6-4-3
49. Najafi A, Nowruzi H, Ghassemi H. Performance prediction of hydrofoil-supported catamarans using experiment and ANNs. Applied Ocean Research. 2018;75:66-84. https://doi.org/10.1016/j.apor.2018.02.017
50. Kazemi H, Doustdar MM, Najafi A, Nowruzi H, Ameri MJ. Hydrodynamic performance prediction of stepped planing craft using CFD and ANNs. Journal of Marine Science and Application. 2021;20:67-84. https://doi.org/10.1007/s11804-020-00182-y
51. Nowruzi H. Performance prediction of stepped planing hulls using experiment and ANNs. Ocean Engineering. 2022;246:110660. https://doi.org/10.1016/j.oceaneng.2022.110660
52. Yousefifard M, Nowruzi H. Hydrodynamic performance of sandglass-type floating body with damping appendages. Ocean Engineering. 2024;309:118579. https://doi.org/10.1016/j.oceaneng.2024.118579
53. Yousefifard M, Maboodi A. Numerical and experimental study of the stern wedge effects on the hydrodynamics performance of a semi-displacement catamaran in calm water. Journal of Applied Fluid Mechanics. 2020;14(2):401-15. https://doi.org/10.47176/jafm.14.02.31361
54. Elsherbiny K. Experimental and numerical analysis of the squat and resistance of ships advancing through the new Suez Canal. 2020.
55. Nazemian A, Ghadimi P. Global optimization of trimaran hull form to get minimum resistance by slender body method. Journal of the Brazilian Society of Mechanical Sciences and Engineering. 2021;43(2):67. https://doi.org/10.1007/s40430-020-02791-8

Persian Abstract

چکیده

برای پیش بینی رفتار کشتی در حالت واقعی دریا، دانستن پاسخ‌های دینامیکی و مقاومتِ افزودهٔ آن در شرایط مختلف فیزیکی و محیطی مهم است. بنابراین، مطالعهٔ حاضر از روش ترکیبی تئوری نواری و دینامیک سیالات محاسباتی برای مطالعه مقاومت افزوده و پاسخ‌های دینامیکی (به عنوان مثال، رائوهای جابجائی عمودی و غلتش طولی) بدنه کشتی دی‌تی‌سی استفاده می‌کند. برای این منظور، طول موج‌ها و جهت‌های مختلف و آبخورها و تریم‌های متفاوت کشتی به عنوان متغیرهای فیزیکی و محیطی تعریف شده در نظر گرفته شده است. علاوه بر این، برای رویکرد دینامیک سیالات محاسباتی، از روش حجم محدود با استفاده از نرم افزار متن‌باز اوپن‌فوم استفاده شد، در حالی که روش تئوری نواری بر مبنای نرم‌افزار ترایبون به‌کار گرفته شده است. نتایج عددی و تئوری نواری در مقابل داده‌های تجربی و عددیِ منتشر شده اعتبارسنجی شده‌اند و مطابقت قابل قبولی حاصل شد. نتایج به‌دست‌آمده نشان می‌دهد که افزایش زوایای موج برخورد کننده با کشتی باعث افزایش رائوی جابجائی عمودی و غلتش طولی می‌شود. علاوه بر این، تغییر آبخور کشتی تأثیر غیر یکنواختی بر افزایش رائو جابجائی عمودی دارد، در حالی که کاهش آبخور باعث افزایش رائو غلتش طولی می‌گردد. همچنین، افزایش تریم به سمت عقب باعث افزایش رائو جابجائی عمودی می‌شود. علاوه بر این، افزایش تریم به سمت سینه، رائو غلتش طولی را افزایش می‌دهد. در نهایت، بیشترین مقدار مقاومت افزوده در حالت موج از روبرو برای آبخورهای کم (۱۲ متر) و تریم معادل ۰/۶ درجه به سمت در حالتی که طول موج برابر با طول کشتی است حاصل می‌شود.